Available online at www.sciencedirect.com
ScienceDirect
Journal of Computational Physics 227 (2008) 4244–4259
JOURNAL OF COMPUTATIONAL PHYSICS
www.elsevier.com/locate/jcp

Numerical upscaling for the eddy-current model with stochastic magnetic materials

Jens P. Eberhard [a,*], Dan Popović [b], Gabriel Wittum [b]

[a] *Computer Simulation Technology, Bad Nauheimer Strasse, 19, D-64289 Darmstadt, Germany*
[b] *Simulation in Technology, University of Heidelberg, Im Neuenheimer Feld 368, D-69120 Heidelberg, Germany*

Received 9 March 2007; received in revised form 19 December 2007; accepted 20 December 2007
Available online 8 January 2008

Abstract

This paper deals with the upscaling of the time-harmonic Maxwell equations for heterogeneous media. We analyze the eddy-current approximation of Maxwell's equations to describe the electric field for heterogeneous, isotropic magnetic materials. The magnetic permeability of the materials is assumed to have random heterogeneities described by a Gaussian random field. We apply the so-called Coarse Graining method to develop a numerical upscaling of the eddy-current model. The upscaling uses filtering and averaging procedures in Fourier space which results in a formulation of the eddy-current model on coarser resolution scales where the influence of sub-scale fluctuations is modeled by effective scale- and space-dependent reluctivity tensors. The effective reluctivity tensors can be obtained by solving local partial differential equations which contain a Laplacian as well as a curl–curl operator. We present a computational method how the equation of the combined operators can be discretized and solved numerically using an extended variational formulation compared to standard discretizations. We compare the results of the numerical upscaling of the eddy-current model with theoretical results of Eberhard [J.P. Eberhard, Upscaling for the time-harmonic Maxwell equations with heterogeneous magnetic materials, Physical Review E 72 (3), (2005)] and obtain a very good agreement.

Keywords: Eddy-current model; Numerical upscaling; Magnetic permeability; Stochastic modeling; Numerical discretization

1. Introduction

Many realistic electromagnetic systems show electric field effects which are strongly influenced by microscopic magnetic parameters of the materials. The phenomena of eddy-currents in heterogeneous magnetic materials is one of the examples where the system behavior depends on the microscopic magnetic permeability distribution. The electromagnetic interactions may take place on very small scales, often of atomistic magnitude. To reduce the computational complexity of the electromagnetic problem we are interested in an

* Corresponding author.
E-mail addresses: jens.eberhard@cst.com (J.P. Eberhard), dan.popovic@stud.uni-heidelberg.de (D. Popović), wittum@uni-hd.de (G. Wittum).

0021-9991/$ - see front matter © 2008 Elsevier Inc. All rights reserved.
doi:10.1016/j.jcp.2007.12.021

upscaling of the eddy-current model onto coarser length scales so that the impact of the sub-scale information need not to be modeled in detail. For the eddy-current model the resulting macroscopic field and current distribution strongly depend on the given magnetic permeability data of the material. However, the detailed magnetic permeability distribution is in most cases not known explicitly. As a solution the magnetic permeability in the eddy-current approximation can be described by the stochastic modeling. The stochastic modeling yields a general approach to handle problems involving heterogeneous materials. It describes an ensemble of realizations of the heterogeneous material by a random field. The material parameter can then be given by a realization of the random field where the values of the realization are explicitly known.

Upscaling for Maxwell's equations has been used for a long time. The use of the mathematical homogenization theory is one of the first approaches which results in averaged or homogenized equations on a coarser scale [20]. For materials with micro-periodic structure a homogenization technique was first introduced in [6,15], where the homogenized material properties have been found by solving local problems by suitable averaging. Heterogeneous composite materials have widely been analyzed, see e.g. [23,24]. A scaling theory for Maxwell's equation concerning composite material was developed in Ref. [31] for the first time. In general, all these homogenization methods have been well analyzed in the literature. For practical applications, however, they may be of limited use due to the more theoretical approach, the requirements of periodic structures, as well as the upscaling to a fixed scale only. For many practical applications, these restrictions may be too far-ranging. Moreover, natural phenomena often need to be modelled by a more realistic way assuming a stochastical distribution for the heterogeneities of the material, where the material characteristics are supposed to be upscaled to various length scales. In this case other upscaling procedures have to be applied. In Ref. [10], a wavelet-base upscaling method was analyzed suitable for non-periodic material. For flow problems an upscaling procedure called Coarse Graining method is well known which allows to perform analytical investigations of heterogeneous media. In the study [11], Eberhard applied the Coarse Graining method for the first time to develop an upscaling for the time-harmonic Maxwell equations with stochastic magnetic materials.

The Coarse Graining method was originally derived in the scope of large eddy simulations and for flow in heterogeneous media, see [25,3,2]. Its basic idea is a splitting and averaging of high-frequency modes in Fourier space. The influence of sub-scale fluctuations is given by effective material parameter tensors. The unique advantage of the Coarse Graining method is that nearly any material can be treated without any restrictions such as periodicity. Also, the scale of the upscaling can be chosen arbitrarily in contrast to the homogenization theory.

The theory of the Coarse Graining method for Maxwell's equations has been analyzed in Ref. [11] where theoretical results for the reluctivity tensors are obtained via a second-order perturbation theory. The numerical computation of these tensors is still lacking, which will be addressed in this paper. We therefore analyze the eddy-current approximation with heterogeneous, isotropic magnetic materials, and we formulate the numerical upscaling based on the Coarse Graining method as shown in Ref. [11]. The upscaling results in effective scale- and space-dependent reluctivity tensors which can be computed by solving local partial differential equations – the so-called sub-problems. Due to the Laplacian and the curl–curl operator these equations are hard to analyze computationally. We present a computational method to discretize the combined operators and to solve them numerically using an extended variational formulation.

The paper is organized as follows. The next section summarizes the physical and mathematical methods to formulate the numerical upscaling. In particular, we introduce the modeling of statistically distributed data with stochastic fields. In Section 3, the theory of the Coarse Graining method for time-harmonic Maxwell equations is introduced as developed by Eberhard [11]. We continue his study and present a numerical approach for the upscaling. To calculate the upscaled material parameters we need to solve local partial differential equations. Section 4 shows the detailed variational formulation and discretization to obtain a computational scheme. In Section 5, we present numerical results of the upscaling and compare them with the theoretical results given by the perturbation theory. We finish with a conclusion and outlook.

2. Definitions and mathematical statement

We briefly describe the mathematical background and the formulation underlying the upscaling for the time-harmonic Maxwell's equation in the eddy-current approximation. In particular, we introduce the

appropriate Sobolev spaces which are used for the variational formulations in the numerical upscaling, and we describe the stochastic modelling for the magnetic permeability used for the resulting Maxwell equation in the eddy-current approximation.

2.1. Sobolev spaces and Green's formulae

Let $\Omega \in \mathbb{R}^3$ be a domain with boundary $\Gamma := \partial\Omega$ equipped with an outwards oriented normal unit field $\mathbf{n}$. We introduce the space $\mathbf{L}^2(\Omega) := (L^2(\Omega))^3$ with the scalar product $\mathbf{u} \cdot \mathbf{v} = (\mathbf{u}, \mathbf{v})_{L^2(\Omega)} := \int_\Omega \mathbf{u}(\mathbf{x})\mathbf{v}(\mathbf{x})\,\mathrm{d}\mathbf{x}$, as done e.g. in Ref. [27]. We remark the difference to the standard scalar product of $\mathbf{L}^2(\Omega)$ which shows a semi-linearity in one of its arguments. The definiton of this scalar product is used due to expressions of the form $\mathbf{a} \cdot \mathbf{E}$, where $\mathbf{a}$ and $\mathbf{E}$ denotes a real and complex vector, respectively.

The Sobolev space $L^\infty(\Omega)$ contains all functions that are bounded in Ω and locally integrable [18]. Further we introduce the following Sobolev spaces,

$$\mathbf{H}(\mathbf{rot};\Omega) := \{\mathbf{u} \in \mathbf{L}^2(\Omega);\ \mathbf{curl}\,\mathbf{u} \in \mathbf{L}^2(\Omega)\},$$
$$\mathbf{H}(\mathrm{div};\Omega) := \{\mathbf{u} \in \mathbf{L}^2(\Omega);\ \mathrm{div}\,\mathbf{u} \in L^2(\Omega)\},$$

where $\mathbf{curl}\,(\cdot)$ and $\mathrm{div}\,(\cdot)$ are set in the weak sense, if necessary [32,7]. For these space we set the following norms, see e.g. [32,7],

$$\|\cdot\|^2_{\mathbf{H}(\mathbf{rot};\Omega)} := \|\cdot\|^2_{\mathbf{L}^2(\Omega)} + (\mathrm{diam}\,\Omega)^2\,\|\mathbf{curl}\,\cdot\|^2_{\mathbf{L}^2(\Omega)},$$
$$\|\cdot\|^2_{\mathbf{H}(\mathrm{div};\Omega)} := \|\cdot\|^2_{\mathbf{L}^2(\Omega)} + (\mathrm{diam}\,\Omega)^2\,\|\mathrm{div}\,\cdot\|^2_{L^2(\Omega)},$$

where the normalization by the diameter of Ω guarantees correct physical units.

On the boundary Γ, we apply special differential operators. We introduce the surface gradient $\mathbf{grad}_\Gamma$ defined by $\mathbf{grad}_\Gamma \Phi|_\Gamma := (\mathbf{grad}\Phi)_\tau$ for a function Φ on $\overline{\Omega}$ with sufficient regularity. $\mathbf{u}_\tau = (\mathbf{u} - (\mathbf{n}\cdot\mathbf{u})\mathbf{n})|_\Gamma = ((\mathbf{n}\times\mathbf{u})\times\mathbf{n})|_\Gamma$ denotes the tangential trace. Analogously the vectorial surface rotation $\mathbf{rot}_\Gamma$ is defined by $\mathbf{rot}_\Gamma \Phi_\Gamma := \mathbf{grad}_\Gamma \Phi|_\Gamma \times \mathbf{n}$. Further, we need the following integration by parts formulae, the so-called *Green's formulae*, for the Laplacian and the **curl curl** operator, see e.g. [32,7].

Let $\mathbf{u} \in \mathbf{H}(\mathbf{rot};\Omega)$. Then $\forall \boldsymbol{\Phi} \in \mathbf{H}^1(\Omega)$

$$\int_\Omega \mathbf{u}\cdot\mathbf{curl}\,\boldsymbol{\Phi} - \mathbf{curl}\,\mathbf{u}\cdot\boldsymbol{\Phi}\,\mathrm{d}\mathbf{x} = \int_{\partial\Omega} \{\mathbf{u}\times\mathbf{n}\}|_\Gamma\,\Phi|_\Gamma\,\mathrm{d}S. \tag{1a}$$

Let $\mathbf{u} \in \mathbf{H}^1(\Omega)$. Then $\forall \boldsymbol{\Phi} \in \mathbf{H}^1(\Omega)$

$$\int_\Omega (\triangle\mathbf{u})\cdot\boldsymbol{\Phi} + (\nabla\mathbf{u})\cdot(\nabla\boldsymbol{\Phi})\,\mathrm{d}\mathbf{x} = \int_{\partial\Omega} (\partial_\mathbf{n}\mathbf{u}|_\Gamma)\cdot\Phi|_\Gamma\,\mathrm{d}\mathbf{n}. \tag{1b}$$

We remark that the boundary integrations over the tangential trace $\{\mathbf{u}\times\mathbf{n}\}|_\Gamma$ and the normal trace $\partial_\mathbf{n}\mathbf{u}|_\Gamma$ respectively are well defined in the dual Sobolev space $\mathbf{H}^{-1/2}(\Gamma)$ of the trace space $\mathbf{H}^{1/2}(\Gamma)$, if $\mathbf{u}$ has sufficient regularity, see [9]. Hence it is also obvious that the boundary integrations have to be interpreted in a weak sense if the functions show lack of requested regularity, see e.g. in [7, Section 5.1.2].

2.2. Stochastic modelling

For the upscaling in the eddy-current approximation we describe the magnetic permeability by a stochastic modelling. The stochastic modelling yields a practical approach to generate realizations of the material so that the quantity of interest can be expressed by explicit values. This approach is based on the assumption that the heterogenities of the data are statistically distributed. In other words, the spatially inhomogeneous distribution of a field $u(\mathbf{x})$ can be identified with a single realization of a stochastic process, defined by the ensemble of all possible realizations, which we assume to be invariant under space transformations. The stochastic modelling approach is in general more suited for practical applications than the standard homogenization method where the material is assumed to have a periodic structure, see e.g. [7,17,20]. The stochastic modelling combined with the Coarse Graining method yields an upscaled model equation along with a variable scale for

the upscaling without the restrictions for the periodicity and the regularity of function spaces as in the homogenization method [2,11,13].

We briefly state the stochastical approach as it can be found, e.g. in Refs. [17,12]. Let $u(\mathbf{x})$, $\mathbf{x} \in \mathbb{R}^3$, be a given homogeneous, ergodic and time-independent scalar random field. Due to the ergodicity the volume average and the ensemble average of the moments of the random field are identical. The field can be divided into its constant mean value $\bar{u}$ and the fluctuations $\tilde{u}(\mathbf{x})$, where $\overline{\tilde{u}(\mathbf{x})} \equiv 0$ holds true. Further, the variance σ_u^2 does not depend on $\mathbf{x}$, and the covariance $\overline{\tilde{u}(\mathbf{x})\tilde{u}(\mathbf{x}')} =: w(\mathbf{x}-\mathbf{x}')$ depends on the distance $\mathbf{x}-\mathbf{x}'$ only. If the Fourier transform of w exists, the correlation function of the Fourier transform of u can be defined by $\overline{\widehat{\tilde{u}}(\boldsymbol{\xi})\,\widehat{\tilde{u}}(\boldsymbol{\xi}')} := \hat{w}(\boldsymbol{\xi},\boldsymbol{\xi}') = (2\pi)^3\,\delta(\boldsymbol{\xi}+\boldsymbol{\xi}')\,\hat{w}(\boldsymbol{\xi})$.

We assume that the correlations of $\tilde{u}(\mathbf{x})$ almost vanish on lengths which are larger than the intrinsic length scales. This fact is modelled, for instance, by choosing a Gaussian correlation function, $w(\mathbf{x}-\mathbf{x}') = \sigma_u^2 \exp(-\sum_{i=1}^{3}(x_i - x_i')^2/(2l_i^2))$. Then, the Gaussian correlation function in Fourier space yields $\hat{w}(\boldsymbol{\xi}) = \sigma_u^2 (2\pi)^{3/2} l_0^3 \exp(-\boldsymbol{\xi}^2 l_0^2/2)$ for isotropic media.

For the numerical generation of the realizations of the random field, we apply an algorithm introduced by Kraichnan [22], see also [12] for a detailed description of the implementation.

2.3. Eddy-current approximation

The fundamental equations modelling electromagnetic field phenomena in a given domain Ω are Maxwell's equations. For the time-harmonic formulation we assume that the current source density $\mathcal{J}$ and the density ρ of free charges are given by harmonic functions, i.e. $\mathcal{J}(\mathbf{x},t) = \mathrm{Re}\,(\mathrm{e}^{\mathrm{i}\omega t}\mathbf{J}(\mathbf{x}))$ and $\rho(\mathbf{x},t) = \mathrm{Re}\,(\mathrm{e}^{\mathrm{i}\omega t} q(\mathbf{x}))$.

This implies that the electric field $\mathcal{E}$ and the magnetic field $\mathcal{H}$ are time-harmonic, see [19]. $\mathbf{J}, q, \mathbf{E}, \mathbf{B}$ and $\mathbf{H}$ are called complex amplitudes of the electromagnetic sources and fields.

The eddy-current approximation for quasi-stationary processes then reads (as shown in [19,7])

$$\mathbf{curl}\, \nu\, \mathbf{curl}\, \mathbf{E} + \mathrm{i}\omega\sigma\mathbf{E} = -\mathrm{i}\omega\mathbf{J}^G, \tag{2}$$

which represents a linear partial differential equation of second order. Eq. (2) assumes that materials located in the domain show linear reactions to impressed fields which yields for the magnetic field $\mathbf{B} = \mu\mathbf{H}$ with the magnetic permeability $\mu(\mathbf{x})$. We also assume Ohm's law $\mathbf{J} = \sigma\mathbf{E} + \mathbf{J}^G$, where σ is the so-called (averaged) conductivity and $\mathbf{J}^G$ is the impressed generator current density. In this study $\mu(\mathbf{x})$ is taken as a scalar field with $\mu > 0$ anywhere, so that the inverse permeability exists and is given by $\mathbf{H} = \nu\mathbf{B}$ where $\nu := \mu^{-1}$ denotes the reluctivity. Further we assume $\sigma \in L^\infty(\Omega)$.

For the uniqueness of the solution it is necessary to specify radiation conditions in infinity, for instance we set uniformly for all directions $\mathbf{x}/|\mathbf{x}|$ the so-called Silver–Müller radiation conditions $\lim_{|x|\to\infty}\big(\sqrt{\mu}\mathbf{x}\times \mathbf{H} + \sqrt{\varepsilon}|\mathbf{x}|\mathbf{E}\big) = 0$ and $\lim_{|x|\to\infty}\big(\sqrt{\epsilon}\mathbf{x}\times\mathbf{E} + \sqrt{\mu}|\mathbf{x}|\mathbf{H}\big) = 0$.

We assume the permeability field $\mu(\mathbf{x})$ to be normal distributed. This, however, conflicts with our assumption $\mu(\mathbf{x}) > 0$ for all $\mathbf{x}$. Therefore, we set-up the field with a mean $\bar{\mu}$ which is at least four times larger than the variance; as a result the probability for a value of $\mu(\mathbf{x}) < 0$ is smaller than 10^{-5} which is sufficient for our computations, see e.g. [28]. This practical approach can be applied if a variable is expected to follow a normal distribution but is restricted to a certain interval such as the positive axis for instance, as described in Ref. [28] for a simple example. We remark that another solution to circumvent this problem would be to consider a truncated normal distribution limited to an interval, see e.g. [26] for a normal distribution limited to positive values.

Let the correlation function as defined in Section 2.2 for $\nu(\mathbf{x})$ be given by its Fourier transform $\overline{\widehat{\tilde{\nu}}(\boldsymbol{\xi})\,\widehat{\tilde{\nu}}(\boldsymbol{\xi}')} = (2\pi)^3\,\bar{\nu}^2\,\hat{w}(\boldsymbol{\xi})\,\delta(\boldsymbol{\xi}+\boldsymbol{\xi}')$, where $\hat{w}(\boldsymbol{\xi})$ denotes an autocorrelation spectrum as introduced in Section 2.2 with isotropic correlation, that is,

$$\hat{w}(\boldsymbol{\xi}) = q_0\,(2\pi)^{\frac{3}{2}}\,l_0^3\,\exp\left(-\frac{1}{2}\boldsymbol{\xi}^2 l_0^2\right). \tag{3}$$

The variance of the field is denoted by q_0 and l_0 is the isotropic correlation length. For the particular case of isotropic fields the correlation function depends on the difference $|\mathbf{x}-\mathbf{x}'|$ only.

3. The coarse graining method

This section describes the Coarse Graining method for the upscaling of the eddy-current approximation as it has been developed in [11]. The key idea of the upscaling method is to transform Eq. (2) first into Fourier space. Second, the electromagnetic field is split into low- and high-frequency solution modes and then averaged over large wave vectors in Fourier space, which correspond to sub-scale oscillations in real space. This upscaling process using the Coarse Graining method results in a formulation of Maxwell's equation (2) on a coarser resolution scale where the impact of the sub-scale fluctuations is given by an effective reluctivity tensor.

Following the ideas of the Coarse Graining method, Eq. (2) will be projected onto high-frequency and low-frequency parts in Fourier space, respectively. As these two parts are coupled the Coarse Graining method decouples them, and after an inverse Fourier transform an upscaled equation akin to (2) on a coarser scale is obtained which includes a effective reluctivity tensor field.

3.1. Upscaling in Fourier space

Starting with Eq. (2) we split the reluctivity field into its mean and the fluctuations, $\nu(\mathbf{x}) = \bar{\nu} + \tilde{\nu}(\mathbf{x})$, and apply $\mathbf{curl}\,\mathbf{curl} = \mathbf{grad}\,\mathrm{div} - \triangle$ as well as $\mathrm{div}\,\mathbf{E} = \rho$. In the latter ρ denotes the free charge distribution varying on macroscopic scales only. We obtain

$$-\bar{\nu}\triangle\mathbf{E}(\mathbf{x}) + \mathbf{curl}\,(\tilde{\nu}(\mathbf{x})\,\mathbf{curl}\,\mathbf{E}(\mathbf{x})) + \mathrm{i}\omega\sigma\mathbf{E}(\mathbf{x}) = \boldsymbol{\gamma}(\mathbf{x}),$$

with a source term $\boldsymbol{\gamma}(\mathbf{x}) := -\mathrm{i}\omega\mathbf{J}^G(\mathbf{x}) - \bar{\nu}\,\mathbf{grad}\,\rho(\mathbf{x})$. This vectorial formulation can be transformed into Fourier space, and regarding the i.th component it yields[1]

$$-\hat{\tilde{\nu}}\sum_{j=1}^{3}(\mathrm{i}\,\xi_j)^2\hat{E}_i(\boldsymbol{\xi}) + \mathrm{i}\omega\sigma\hat{E}_i(\boldsymbol{\xi}) + \epsilon_{ijk}\epsilon_{klm}\mathrm{i}\xi_j\int\hat{\tilde{\nu}}(\boldsymbol{\xi}-\boldsymbol{\xi}')\mathrm{i}\xi'_l\hat{E}_m(\boldsymbol{\xi}')\,\mathrm{d}^3\xi' = \hat{\gamma}_i(\boldsymbol{\xi}). \tag{4}$$

Next, we define analogously to [11] (see Eq. (6) in there)

$$R_{jl}(\boldsymbol{\xi},\boldsymbol{\xi}') := \mathrm{i}\,\xi_j\,\hat{\tilde{\nu}}(\boldsymbol{\xi}-\boldsymbol{\xi}')\,\mathrm{i}\,\xi'_l \quad\text{and}\quad g_0(\boldsymbol{\xi}) := \left(-\bar{\nu}\sum_j(\mathrm{i}\,\xi_j)^2 + \mathrm{i}\,\omega\,\sigma\right)^{-1}.$$

Hence (4) becomes

$$g_0^{-1}(\boldsymbol{\xi})\,\hat{E}_i(\boldsymbol{\xi}) + \epsilon_{ijk}\epsilon_{klm}\int R_{jl}(\boldsymbol{\xi},\boldsymbol{\xi}')\hat{E}_m(\boldsymbol{\xi}')\,\mathrm{d}^3\xi' = \hat{\gamma}_i(\boldsymbol{\xi}). \tag{5}$$

We assume that the dyadic Green's function for problem (5) in Fourier space exists, see e.g. [30]. Then $\hat{G}_{m\eta}(\boldsymbol{\xi},\boldsymbol{\xi}')$ satisfies for fixed component i and fixed column index η

$$\begin{aligned} &g_0^{-1}(\boldsymbol{\xi})\,\hat{G}_{i\eta}(\boldsymbol{\xi},\boldsymbol{\xi}') + \textstyle\int\epsilon_{ijk}\,\epsilon_{klm}\,R_{jl}(\boldsymbol{\xi},\boldsymbol{\xi}'')\,\hat{G}_{m\eta}(\boldsymbol{\xi}'',\boldsymbol{\xi}')\,\mathrm{d}^3\xi'' = (\delta(\boldsymbol{\xi}+\boldsymbol{\xi}')\,\mathbf{e}_\eta)_i \\ \iff &\textstyle\int(g_0^{-1}(\boldsymbol{\xi}'')\,\delta_{im}\,\delta(\boldsymbol{\xi}-\boldsymbol{\xi}'') + \epsilon_{ijk}\,\epsilon_{klm}\,R_{jl}(\boldsymbol{\xi},\boldsymbol{\xi}''))\,\hat{G}_{m\eta}(\boldsymbol{\xi}'',\boldsymbol{\xi}')\,\mathrm{d}^3\xi'' = \delta(\boldsymbol{\xi}+\boldsymbol{\xi}')\,\delta_{i\eta}. \end{aligned}$$

In this definition the summation is given over j,k,l and m. δ_{im} denotes the Kronecker delta, $\delta(\boldsymbol{\xi}\pm\boldsymbol{\xi}')$ a delta distribution [16] and $\mathbf{e}_{(\cdot)}$ a basis vector. The definition states an equation system for each column of the dyadic Green's function. Further, a series expansion of $\hat{G}_{m\eta}$ in g_0 can be derived, see e.g. [11]. Eberhard [11] also shows that if the fluctuations in Fourier space vanish, $\hat{\tilde{\nu}}(\boldsymbol{\xi}) \equiv 0$, $\hat{G}_{m\eta}(\boldsymbol{\xi},\boldsymbol{\xi}')$ has diagonal form.

According to the Coarse Graining method in [11] we define projectors in Fourier space which divide the field vector in high- and low-frequency parts:

[1] Throughout this section, the $\boldsymbol{\xi}$-dependence is denoted for the fluctuations of the reluctivity field only.

$$P^{+}_{\lambda,\xi}[\widehat{\mathbf{E}}(\boldsymbol{\xi})] := \begin{cases} \widehat{\mathbf{E}}(\boldsymbol{\xi}) & \text{if } |\xi_i| > \frac{a_s}{\lambda} \quad \text{for one } i \in I, \\ 0 & \text{else,} \end{cases}$$
$$P^{-}_{\lambda,\xi}[\widehat{\mathbf{E}}(\boldsymbol{\xi})] := \begin{cases} \widehat{\mathbf{E}}(\boldsymbol{\xi}) & \text{if } |\xi_i| \leqslant \frac{a_s}{\lambda} \quad \forall i \in I, \\ 0 & \text{else,} \end{cases} \tag{6}$$

where $I = \{1, 2, 3\}$ and a_s is a constant. If necessary we use the abbreviation $P^{+}_{\lambda,\xi,\xi'}[\widehat{\mathbf{E}}(\boldsymbol{\xi})]$ instead of $P^{+}_{\lambda,\xi}[P^{+}_{\lambda,\xi'}[\widehat{\mathbf{E}}(\boldsymbol{\xi})]]$ or omit the indices. This holds true for P^{-}, too. We can project the Fourier transform $\widehat{\mathbf{E}}$ of the solution

$$\widehat{\mathbf{E}}(\boldsymbol{\xi}) = P^{+}_{\lambda,\xi}[\widehat{\mathbf{E}}(\boldsymbol{\xi})] + P^{-}_{\lambda,\xi}[\widehat{\mathbf{E}}(\boldsymbol{\xi})]$$

and Eq. (5) as well,

$$P^{+}_{\lambda,\xi}[g_0^{-1}\widehat{E}_i(\boldsymbol{\xi})] - P^{+}_{\lambda,\xi}\left[\epsilon_{ijk}\epsilon_{klm}\int R_{jl}(\boldsymbol{\xi},\boldsymbol{\xi}')\widehat{E}_m(\boldsymbol{\xi}')\,\mathrm{d}^3\xi'\right] = P^{+}_{\lambda,\xi}[\hat{\gamma}_i(\boldsymbol{\xi})].$$

For $P^{-}_{\lambda,\xi}$ we get an analogous expression. It is obvious that the expressions for $P^{+}[\widehat{E}_i(\boldsymbol{\xi})]$ and $P^{-}[\widehat{E}_i(\boldsymbol{\xi})]$ are coupled due to the contained convolution. The decoupling idea of the Coarse Graining method is to find a closed expression for $P^{-}[\widehat{E}_i(\boldsymbol{\xi})]$ which contains low-frequency components only. This expression corresponds in real space to a quantity that contains components with period lengths larger than λ. Oscillations of period lengths smaller than λ are in Fourier space represented by $P^{+}[\widehat{E}_i(\boldsymbol{\xi})]$. As a result, the method first decouples both parts and then inserts $P^{+}[\widehat{E}_i(\boldsymbol{\xi})]$ into the expression for $P^{-}[\widehat{E}_i(\boldsymbol{\xi})]$ to gain a closed expression for $P^{-}[\widehat{E}_i(\boldsymbol{\xi})]$. The decoupling idea is described in detail by Eberhard [11] where the upscaling is performed including all mathematical steps. The resulting upscaling models the influences of the sub-scale fluctuations by a scale-dependent tensor quantity $\delta v^{\mathrm{eff}}(\boldsymbol{\xi}, \lambda)$ which incorporates the impact of the unresolved fluctuations [11]:

$$\delta v^{\mathrm{eff}}_{kr}(\boldsymbol{\xi}, \lambda) = \frac{\epsilon_{klm}}{(2\pi)^6}\iint \overline{\widehat{\tilde{v}}(\boldsymbol{\xi} - \boldsymbol{\xi}')\mathrm{i}\xi'_l P^{+}_{\lambda,\xi'\xi''}\widehat{G}_{mn}(\boldsymbol{\xi}', -\boldsymbol{\xi}'')\epsilon_{npr}\mathrm{i}\,\xi''_p\widehat{\tilde{v}}(\boldsymbol{\xi}'' - \boldsymbol{\xi})}\,\mathrm{d}^3\xi''\,\mathrm{d}^3\xi',$$

where λ denotes the upscaling scale which is determined by the definition of the projections in Fourier space, see Eq. (6). $\delta v^{\mathrm{eff}}(\boldsymbol{\xi}, \lambda)$ is called *effective reluctivity tensor*. We remark that the Coarse Graining method leads to a tensor field on the coarser scale, even if the field on the fine scale is a scalar field. In $\delta v^{\mathrm{eff}}(\boldsymbol{\xi}, \lambda)$ the summation is taken over l, m, n and p, while k and r are fixed. $\delta v^{\mathrm{eff}}(\boldsymbol{\xi}, \lambda)$ corresponds in real space to a non-local quantity. For a localization it is evaluated for $\boldsymbol{\xi} = 0$ [11]. Thus, as an approximation we can set $\delta v^{\mathrm{eff}}_{kr}(\boldsymbol{\xi}, \lambda) \approx \delta v^{\mathrm{eff}}_{kr}(\boldsymbol{\xi} = 0, \lambda) := \delta v^{\mathrm{eff}}_{kr}(\lambda)$, which leads to

$$\delta v^{\mathrm{eff}}_{kr}(\lambda) := \frac{\epsilon_{klm}}{(2\pi)^6}\iint \overline{\widehat{\tilde{v}}(-\boldsymbol{\xi}')\mathrm{i}\xi'_l P^{+}_{\lambda,\xi'}[P^{+}_{\lambda,\xi''}\widehat{G}_{mn}(\boldsymbol{\xi}', -\boldsymbol{\xi}'')]\epsilon_{npr}\mathrm{i}\,\xi''_p\widehat{\tilde{v}}(\boldsymbol{\xi}'')}\,\mathrm{d}^3\xi''\,\mathrm{d}^3\xi'. \tag{7}$$

After an inverse Fourier transform we get an upscaled formulation of Eq. (2) in real space on the scale λ,

$$\mathbf{curl}\,(\bar{v} - \delta v^{\mathrm{eff}}_{kr}(\lambda) + \tilde{v}(\mathbf{x})|_\lambda)\,\mathbf{curl}\,\mathbf{E}|_\lambda + \mathrm{i}\omega\sigma\mathbf{E}|_\lambda = \mathrm{i}\omega\mathbf{J}^G|_\lambda, \tag{8}$$

where only the indices of the effective reluctivity are depicted to clarify that it is a tensor. In this model, the quantities $\mathbf{J}^G|_\lambda$, $\tilde{v}(\mathbf{x})|_\lambda$, and the solution $\mathbf{E}|_\lambda$ are upscaled to the scale λ. All fine-scale information is incorporated into the effective reluctivity tensor $\delta v^{\mathrm{eff}}(\lambda)$. On scale λ the scalar sub-scale reluctivity field becomes a reluctivity tensor field which is made of the space-independent ensemble mean, the upscaled fluctuations and the effective reluctivity from the Coarse Graining method. The total effective tensor on λ can then defined by

$$v^{\mathrm{eff}}(\lambda) := \bar{v} - \delta v^{\mathrm{eff}}_{kr}(\lambda). \tag{9}$$

In the case of small variances q_0 in (3), that is, weak heterogeneity, a perturbation theory approach can be deployed to obtain an explicit result for v^{eff} [11]. The numerical computation of (9) will be regarded in Section 4.

3.2. Perturbation theory for $\delta\nu^{\text{eff}}$

In Ref. [11] $\delta\nu^{\text{eff}}(\lambda)$ is calculated with the aid of perturbation theory. The results are valid for weakly heterogeneous reluctivity fields $\nu(\mathbf{x})$ on the fine scale, i.e. if the variance q_0 in the correlation function (3) is small, $q_0 \ll 1$. The integrations for $\delta\nu^{\text{eff}}(\lambda)$ are treated using smooth cut off functions instead of the sharp projectors in Fourier space, $P^{+}_{\lambda,\xi} \to [1 - \exp(-\boldsymbol{\xi}^2\lambda^2/(2a_w^2))]$, see [11]. It is shown in [11] that the non-diagonal entries of the effective reluctivity tensor vanish and the integrations for the diagonal is given by

$$\delta\nu^{\text{eff}}_{kk}(\lambda) = \frac{\sqrt{2}q_0 l_0^3 \bar{\nu}}{3}\left[M\left(\frac{l_0^2}{2}, \omega\sigma\right) - M\left(l_0^2 + \frac{\lambda^2}{2a_w^2}, \omega\sigma\right)\right], \tag{10}$$

where the function $M(a,b)$ is defined by

$$M(a,b) := \frac{1}{2a^{3/2}} - \frac{\mathrm{i}b}{\bar{\nu}\sqrt{a}} + \frac{\sqrt{\pi}b^{3/2}}{\bar{\nu}^{3/2}}(-1)^{3/4}\exp\left(\frac{\mathrm{i}ab}{\bar{\nu}}\right)\operatorname{erfc}\left(\sqrt{\mathrm{i}ab/\bar{\nu}}\right).$$

Here erfc denotes the complex error function as defined, e.g. in [1].

3.3. Approximation of $\delta\nu^{\text{eff}}$ in real space

Next we briefly conclude how $\delta\nu^{\text{eff}}(\lambda)$ is transformed to real space, as it is shown in [11]. In the case of a global upscaling, $\lambda \to \infty$, all fluctuations are eliminated, and a constant value for the scalar reluctivity is obtained, see [11], Appendix B.

For the upscaling to finite length scales, $\lambda < \infty$, the derivation is more complicated due to the projection in definition (7) of $\delta\nu^{\text{eff}}_{kr}(\lambda)$. This projection can be seen as a characteristic function in Fourier space and hence becomes a distribution S in real space (see [11]), with

$$S(\mathbf{x},\lambda) = \frac{1}{(2\pi)^3}\int \mathrm{e}^{\mathrm{i}\boldsymbol{\xi}\cdot\mathbf{x}} P^{+}_{\lambda,\xi}\,\mathrm{d}^3\xi.$$

The analysis in [11] yields the following asymptotics: $S(\mathbf{x},0) \approx 0$ for $\lambda \to 0$ and $S(\mathbf{x},\lambda) \approx \delta(\mathbf{x})$ for $\lambda \to \infty$. With this distribution definition (7) of the effective reluctivity tensor yields after an inverse Fourier transform

$$\delta\nu^{\text{eff}}_{kr}(\lambda) = \epsilon_{klm}\int \overline{\tilde{\nu}(\mathbf{x})S(\mathbf{x}-\mathbf{x}',\lambda)\partial_{x_l'}G_{mn}(\mathbf{x}',\mathbf{x}'')\epsilon_{npr}\,S(\mathbf{x}''-\mathbf{x}''',\lambda)\partial_{x_p'''}\tilde{\nu}(\mathbf{x}''')}\mathrm{d}^3x''' \cdots \mathrm{d}^3x.$$

A further approximation has to be introduced similar as in the case of upscaling of flow in heterogeneous media, see [13]. The idea is that $S(\cdot,\cdot)$ acts locally as a smoother when it is folded with a function with compact support. Hence the impact of S together with an integration can be approximated by an averaging over a local volume $\Omega_\lambda^{(\mathbf{x})}$, which is proportional to the scale λ. Therefore we define the three-dimensional cube

$$\Omega_\lambda^{(\mathbf{x})} := \prod_{i=1}^{3}[x_i - \lambda/a_s, x_i + \lambda/a_s]$$

surrounding the point $\mathbf{x}$. Due to the folding with the distribution the effective reluctivity tensor localized in the sub-volume $\Omega_\lambda^{(\mathbf{x})}$ reads

$$\delta\nu^{\text{eff}}_{kr}(\lambda,\mathbf{x}) \approx \epsilon_{klm}\int \overline{\tilde{\nu}(\mathbf{x})\,\partial_{x_l}\left(\int_{\Omega_\lambda^{(\mathbf{x})}} G_{mn}(\mathbf{x},\mathbf{x}')\,\epsilon_{npr}\,\partial_{x_p'}\tilde{\nu}(\mathbf{x}')\right)}\,\mathrm{d}^3x'\,\mathrm{d}^3x. \tag{11}$$

For $\lambda = 0$ and $\lambda \to \infty$ the approximation yields the exact effective reluctivity from (11), see [11]. So far, the computation of $\delta\nu^{\text{eff}}(\lambda)$ contains an ensemble average. For numerical computations it is useful to refer to an effective reluctivity for a single realization where the tensor can be gained by the information of this single realization. For this case the single realization tensor $\delta\nu^{\text{real}}$ can be defined analogously to (11), but without the ensemble mean, so that $\delta\nu^{\text{eff}}(\lambda) = \overline{\delta\nu^{\text{real}}(\lambda)}$ holds true.

Finally, we derive a partial differential equation which can be applied to compute the reluctivity tensor (11) numerically. To calculate the tensor we need to know Green's function $G_{m\eta}(\mathbf{x},\mathbf{x}')$ and to sum over its columns $G_{\cdot\eta}$. Due to the local integrations over the sub-volumes $\Omega_\lambda^{(\mathbf{x})}$ an approximation of G by a local Green's function is obvious, see [11].

In $\Omega_\lambda^{(\mathbf{x})}$ the local Green's function $G^{(\mathbf{x})}_{m\eta}(\mathbf{x}',\mathbf{x}'')$, where $\mathbf{x}$ is the index depicting the specific volume where the tensor has to be calculated, can be defined by ($\mathbf{x}$ is fixed, the operators are acting on $\mathbf{x}'$)

$$-\bar{\nu}\sum_{j=1}^{3}\partial^2_{x'_j}\delta_{im}G^{(\mathbf{x})}_{m\eta}(\mathbf{x}',\mathbf{x}'')+\mathrm{i}\omega\sigma\delta_{im}G^{(\mathbf{x})}_{m\eta}(\mathbf{x}',\mathbf{x}'')+\epsilon_{ijk}\epsilon_{klm}\partial_{x'_j}\tilde{\nu}(\mathbf{x}')\partial_{x'_l}G^{(\mathbf{x})}_{m\eta}(\mathbf{x}',\mathbf{x}'')=\delta(\mathbf{x}'-\mathbf{x}'')\delta_{i\eta} \tag{12}$$

in $\Omega_\lambda^{(\mathbf{x})}$ which implies a single equation system for each column indexed by $\eta=1,2,3$. The boundary conditions for (12) will be specified in Section 4.

As a result, the local reluctivity tensor $\delta\nu^{\mathrm{eff}}_{kr}(\lambda)$ from definition (11) can for a single realization be calculated by

$$\delta\nu^{\mathrm{real}}_{kr}(\lambda,\mathbf{x}):=\int\epsilon_{klm}\tilde{\nu}(\mathbf{x}')\partial_{x'_l}\int_{\Omega_\lambda^{(\mathbf{x})}}G^{(\mathbf{x})}_{mn}(\mathbf{x}',\mathbf{x}'')\epsilon_{npr}\,\partial_{x''_p}\tilde{\nu}(\mathbf{x}'')\,\mathrm{d}^3x''\,\mathrm{d}^3x'. \tag{13}$$

For simplifications, we define

$$\mathcal{X}^{(\mathbf{x})}_{mr}(\mathbf{x}'):=\int_{\Omega_\lambda^{(\mathbf{x})}}G^{(\mathbf{x})}_{mn}(\mathbf{x}',\mathbf{x}'')\epsilon_{npr}\partial_{x''_p}v(\mathbf{x}'')\,\mathrm{d}^3x'', \tag{14}$$

where the indices m and r are fixed. Since we sum over q the index n is uniquely determined. The function $\mathcal{X}$ satisfies an equation which is obtained multiplying Eq. (12) with $\epsilon_{npr}\partial_{\mathbf{x}''_p}\tilde{\nu}(\mathbf{x}'')$, where η is replaced by n, summing over the columns of the local Green's function, and integrating. It yields for fixed index i for each of the independent three columns of $\mathcal{X}$, $\mathcal{X}^{(x)}_{\cdot r}$

$$-\bar{\nu}\triangle\mathcal{X}^{(\mathbf{x})}_{ir}(\mathbf{x}')+\mathrm{i}\omega\sigma\mathcal{X}^{(\mathbf{x})}_{ir}(\mathbf{x}')+[\mathbf{curl}\,\tilde{\nu}(\mathbf{x}')\,\mathbf{curl}\,\mathcal{X}^{(\mathbf{x})}_{\cdot r}(\mathbf{x}')]_i=\epsilon_{ipr}\,\partial_{x'_p}\,\tilde{\nu}(\mathbf{x}'). \tag{15}$$

Eq. (15) has to be solved for the three indices $r=1,2,3$ numerically. Accordingly, if $\mathcal{X}$ is known the reluctivity tensor can be calculated numerically via

$$\delta\nu^{\mathrm{num}}_{kr}(\lambda,\mathbf{x}')=\int_{\Omega_\lambda^{(\mathbf{x})}}\epsilon_{klm}\,\tilde{\nu}(\mathbf{x}')\,\partial_{x'_l}\,\mathcal{X}^{(\mathbf{x})}_{mr}(\mathbf{x}')\,\mathrm{d}^3x'. \tag{16}$$

4. Numerical coarse graining

In this section, we will establish a variational formulation for Eq. (15) and show how a discretization using a standard Galerkin method can be set up numerically.

4.1. Variational formulation

For the numerical Coarse Graining we refer to the three-dimensional unit cube, $\Omega=[0,1]^3$. We provide a partition of Ω with a cubic grid including $d\in\mathbb{N}$ cubes on one edge of Ω, and a stochastical permeability field $\mu(\mathbf{x})$ which has constant values on the cubes of the grid. As a result, the reluctivity field $\nu(\mathbf{x})$ can be obtained by element-wise inversion.

We fix the length scale λ to an arbitrary value for the upscaling. In the unit cube with the given reluctivity field, we join several reluctivity cells to one block, in that way that each block is a cube again. Then the scale λ is defined by the number of reluctivity cells we merge.

Eq. (15) is governed by a differential operator of the form

$$\mathbf{curl}\,\tilde{\nu}(\mathbf{x})\,\mathbf{curl}+\mathbf{Id}+\bar{\nu}\triangle. \tag{17}$$

To our knowledge, a stable discretization for this type of operator is not yet known. The main problem is to find an appropriate space for a variational formulation. This is due to the fact that the Laplace operator

cannot be handled with a variational formulation over the space $\mathbf{H}(\mathbf{rot};\Omega)$, which is usually the appropriate space for equations containing the **curl curl** operator, see e.g. [7].

On the other hand, the **curl curl** operator cannot be discretized by $\mathbf{H}^1(\Omega)$-conforming finite elements since $\mathbf{H}^1(\Omega)$ is a closed subspace of $\mathbf{H}(\mathbf{rot};\Omega)$. It is well known that a treatment of **curl curl** equations by a $\mathbf{H}^1(\Omega)$-conforming FEM leads to singularities of the solutions at re-entrant corners, which are not covered by $\mathbf{H}^1(\Omega)$, see e.g. [9].

But for convex domains it is well known that the spaces $\mathbf{X}_N(\Omega) := \mathbf{H}^1(\mathrm{div};\Omega) \cap \mathbf{H}(\mathbf{curl};\Omega)$ and $\mathbf{H}_N(\Omega) := \{\mathbf{v} \in \mathbf{H}^1;\ \mathbf{v}\times\mathbf{n} = 0 \text{ on } \partial\Omega\}$ coincide, see [8] and the therein given references.

Since the choice of the Coarse Graining blocks $\Omega_\lambda^{(\mathbf{x})}$ as stated above leads to convex domains, we analyze if a treatment of the local Coarse Graining problems in form of Eq. (15) with $\mathbf{H}^1$-conforming finite elements is possible.

We start with the vectorial form (15) of the additional equation for $\mathcal{X}$:

$$-\bar{\nu}\triangle\mathcal{X}_{\cdot r}^{(\mathbf{x})}(\mathbf{x}') + \mathrm{i}\omega\sigma\mathcal{X}_{\cdot r}^{(\mathbf{x})}(\mathbf{x}') + \mathbf{curl}\,\tilde{\nu}(\mathbf{x}')\,\mathbf{curl}\,\mathcal{X}_{\cdot r}^{(\mathbf{x})}(\mathbf{x}') = \epsilon_{\cdot pr}\partial_{x'_p}\tilde{\nu}(\mathbf{x}'). \tag{18}$$

Again $r = 1,2,3$ indicates the columns of $\mathcal{X}$. We study two different boundary conditions. Since the Laplacian dominates the equation, we firstly choose Dirichlet boundary conditions on $\partial\Omega_\lambda^{(\mathbf{x})}$,

$$\begin{aligned}&\mathcal{X}_{\cdot r}^{(\mathbf{x})}(\mathbf{x}') = 0, \text{ and secondly}\\ &\mathbf{n}(\mathbf{x}')\times\mathcal{X}_{\cdot r}^{(\mathbf{x})}(\mathbf{x}') = 0\end{aligned} \tag{19}$$

due to the convex domain argument, with $\mathbf{n}(\mathbf{x}')$ denoting the unit normal field for $\Omega_\lambda^{(\mathbf{x})}$. We define

$$\boldsymbol{\mathcal{W}}(\Omega_\lambda^{(\mathbf{x})}) := \{\mathbf{v} \in \mathbf{H}^1(\Omega_\lambda^{(\mathbf{x})}),\ \mathbf{v} \text{ satisfies the chosen boundary condition}\},$$

which leads to $\boldsymbol{\mathcal{W}} = \mathbf{H}_0^1$ or $\boldsymbol{\mathcal{W}} = \mathbf{H}_N$. Testing with functions $\boldsymbol{\psi}$ from $\boldsymbol{\mathcal{W}}(\Omega_\lambda^{(\mathbf{x})})$ and applying the partial integration formulae (1a) for the **curl curl** and (1b) for the Laplacian, we obtain

$$\begin{aligned}&\int_{\Omega_\lambda^{(\mathbf{x})}} \bar{\nu}\{\nabla\mathcal{X}_{\cdot r}^{(\mathbf{x})}(\mathbf{x}')\}\cdot\nabla\boldsymbol{\psi}(\mathbf{x}')\,\mathrm{d}\mathbf{x}' + \int_{\Omega_\lambda^{(\mathbf{x})}} \tilde{\nu}(\mathbf{x}')\,\mathbf{curl}\,\mathcal{X}_{\cdot r}^{(\mathbf{x})}(\mathbf{x}')\cdot\mathbf{curl}\,\boldsymbol{\psi}(\mathbf{x}')\,\mathrm{d}\mathbf{x}'\\ &- \int_{\partial\Omega_\lambda^{(\mathbf{x})}} \{\partial_n\mathcal{X}_{\cdot r}^{(\mathbf{x})}\}\cdot\boldsymbol{\psi}(\mathbf{x}')\,\mathrm{d}S - \int_{\partial\Omega_\lambda^{(\mathbf{x})}} \{\{\tilde{\nu}(\mathbf{x}')\mathbf{curl}\,\mathcal{X}_{\cdot r}^{(\mathbf{x})}(\mathbf{x}')\}\times\mathbf{n}\}\cdot\boldsymbol{\psi}(\mathbf{x}')\,\mathrm{d}S\\ &+ \int_{\Omega_\lambda^{(\mathbf{x})}} \mathrm{i}\,\omega\,\sigma\,\mathcal{X}_{\cdot r}^{(\mathbf{x})}(\mathbf{x}')\cdot\boldsymbol{\psi}(\mathbf{x}')\,\mathrm{d}\mathbf{x}' = \int_{\Omega_\lambda^{(\mathbf{x})}} \{\epsilon_{\cdot pr}\,\partial_{x'_p}\,\tilde{\nu}(\mathbf{x}')\}\cdot\boldsymbol{\psi}(\mathbf{x}')\,\mathrm{d}\mathbf{x}', \quad \forall\boldsymbol{\psi} \in \boldsymbol{\mathcal{W}}(\Omega_\lambda^{(\mathbf{x})}).\end{aligned}$$

In the following the curled braces $\{\cdot\}$ also denote vectors. As natural boundary conditions we set $\int\{\partial_{\mathbf{n}}\mathcal{X}_{\cdot r}\}\cdot\boldsymbol{\psi}\,\mathrm{d}S = 0$ and $\int\{\{\tilde{\nu}(\mathbf{x}')\,\mathbf{curl}\,\mathcal{X}_{\cdot r}\}\times\mathbf{n}\}\cdot\boldsymbol{\psi}\,\mathrm{d}S = 0$, where the derivation $\partial_{\mathbf{n}}$ is in the direction of the normal unit. The problem then yields:

Find a function $\mathcal{X}_{\cdot r}^{(\mathbf{x})}$ in $\boldsymbol{\mathcal{W}}(\Omega_\lambda^{(\mathbf{x})})$, such that for all $\boldsymbol{\psi} \in \boldsymbol{\mathcal{W}}(\Omega_\lambda^{(\mathbf{x})})$

$$a(\mathcal{X}_{\cdot r}^{(\mathbf{x})}, \boldsymbol{\psi}) = \langle \boldsymbol{I}, \boldsymbol{\psi}\rangle, \tag{20}$$

with the Sesqui-linear form

$$\begin{aligned}a(\mathcal{X}_{\cdot r}^{(\mathbf{x})}, \boldsymbol{\psi}) := &\int_{\Omega_\lambda^{(\mathbf{x})}} \bar{\nu}\{\nabla\mathcal{X}_{\cdot r}^{(\mathbf{x})}(\mathbf{x}')\}\cdot\nabla\boldsymbol{\psi}(\mathbf{x}')\,\mathrm{d}\mathbf{x}' + \int_{\Omega_\lambda^{(\mathbf{x})}} \mathrm{i}\,\omega\,\sigma\,\mathcal{X}_{\cdot r}^{(\mathbf{x})}(\mathbf{x}')\cdot\boldsymbol{\psi}(\mathbf{x}')\,\mathrm{d}\mathbf{x}'\\ &+ \int_{\Omega_\lambda^{(\mathbf{x})}} \tilde{\nu}(\mathbf{x}')\,\mathbf{curl}\,\mathcal{X}_{\cdot r}^{(\mathbf{x})}(\mathbf{x}')\cdot\mathbf{curl}\,\boldsymbol{\psi}(\mathbf{x}')\,\mathrm{d}\mathbf{x}'\end{aligned}$$

and the dual product $\langle \boldsymbol{I}, \boldsymbol{\psi}\rangle_{\boldsymbol{\mathcal{W}}'\times\boldsymbol{\mathcal{W}}} := \int_{\Omega_\lambda^{(\mathbf{x})}} \{\epsilon_{\cdot pr}\,\partial_{x'_p}\,\tilde{\nu}(\mathbf{x}')\}\cdot\boldsymbol{\psi}(\mathbf{x}')\,\mathrm{d}\mathbf{x}'$.

4.2. Domain triangulation and Galerkin method

We choose a consistent triangulation $\mathcal{T}^h$ of the volume $\Omega_\lambda^{(\mathbf{x})}$ using tetrahedra. The unknowns are located in the corner of the element nodes. The set of nodes is denoted by $\mathcal{N}_N$ and we set $N_N := |\mathcal{N}_N|$. An iterative

regular refinement gives a hierarchy $\mathcal{T}^l,\ l = 0,\ldots,L$ of nested consistent tetrahedral triangulations, 0 labeling the coarsest level. Due to the regular refinement strategy the family of triangulations $(\mathcal{T}^h)_h$ is stable.

We apply a standard Galerkin method for the problem. As a finite dimensional subspace of $\boldsymbol{\mathcal{W}}$ we set

$$\mathcal{S}^h := \{f \in C(\Omega_\lambda^{(\mathbf{x})});\quad f \text{ is linear on each tetrahedra and satisfies the boundary condition from (19)}\},$$

and $\boldsymbol{\mathcal{S}}^h := (\mathcal{S}^h)^3$.

Problem (20) then reads: find $\mathcal{X}_{\cdot r}^{(x),h}$ in $\boldsymbol{\mathcal{S}}^h$, such that for all $\boldsymbol{\psi}$ in $\boldsymbol{\mathcal{S}}^h$

$$a(\mathcal{X}_{\cdot r}^{(\mathbf{x}),h}, \boldsymbol{\psi}) = \langle \boldsymbol{l}, \boldsymbol{\psi}\rangle. \tag{21}$$

A basis $\{\boldsymbol{\varphi}_1^i, \boldsymbol{\varphi}_2^i, \boldsymbol{\varphi}_3^i\},\ i = 1,\ldots,N_N$ for $\boldsymbol{\mathcal{S}}^h$ can in each node $\mathbf{y}^i$ be set as follows:

$$\boldsymbol{\varphi}_1^i(\mathbf{y}^i) = \varphi^i(\mathbf{y}^i)\,\mathbf{e}_1, \quad \boldsymbol{\varphi}_2^i(\mathbf{y}^i) = \varphi^i(\mathbf{y}^i)\,\mathbf{e}_2, \quad \boldsymbol{\varphi}_3^i(\mathbf{y}^i) = \varphi^i(\mathbf{y}^i)\,\mathbf{e}_3,$$

with the standard scalar shape functions $\varphi : \mathbb{R}^3 \mapsto \mathbb{R}$ and the canonical basis vectors $\mathbf{e}_{(\cdot)}$. As a result, the total number of test functions is $3N_N$ and $dim\,\boldsymbol{\mathcal{S}}^h = 3N_N$. With this basis the unknown functions $\mathcal{X}^h \cdot r(\mathbf{x}')$ are given by $(r = 1,2,3)$:

$$\mathcal{X}_{\cdot r}^{(\mathbf{x})\,h}(\mathbf{x}') = \sum_{j=1}^{N_N} z_1^j \boldsymbol{\varphi}_1^j(\mathbf{x}') + z_2^j \boldsymbol{\varphi}_2^j(\mathbf{x}') + z_3^j \boldsymbol{\varphi}_3^j(\mathbf{x}') = \sum_{j=1}^{N_N} z_1^j\,\varphi^j(\mathbf{x}')\,\mathbf{e}_1 + z_2^j\,\varphi^j(\mathbf{x}')\,\mathbf{e}_2 + z_3^j\,\varphi^j(\mathbf{x}')\,\mathbf{e}_3. \tag{22}$$

The weights z_d^j are complex-valued for all $j \in 1,\ldots,N_N$ and $d = 1,2,3$. We abbreviate the vectors of nodal unknowns by $\tilde{\mathbf{z}}_d = (z_d^j)_j, d = 1,2,3$. Finally problem (21) yields:

Find $\mathcal{X}_{\cdot r}^{(x),h}$ in $\boldsymbol{\mathcal{S}}^h$, such that for all $i = 1,\ldots,N_N$:

$$a(\mathcal{X}_{\cdot r}^{(\mathbf{x}),h}, \boldsymbol{\varphi}_d^i) = \langle \boldsymbol{l}, \boldsymbol{\varphi}_d^i\rangle, \tag{23}$$

for each of the three basis vectors $\boldsymbol{\varphi}_d,\ d = 1,2,3$.

4.3. Assembling the system matrix

The assembling proceeds analogously to the case of discretizing Maxwell's equations applying a vector potential formulation with unknown values in the nodes as it is shown e.g. in [21]. Insertion of $\mathcal{X}_{\cdot r}$ expressed by (22) into (23) leads to the discrete equation system where we get three equations for the three components of each column vector $\mathcal{X}_{\cdot r}$. While the assembling of the system matrix does not depend on the column index of $\mathcal{X}$, the right-hand side discretization will differ with r as shown in Section 4.4.

We execute the assembling of the first component $(i = 1)$ for $\boldsymbol{\varphi}_1$ explicitly (r fixed).

This results in the following problem: Search complex weights $\tilde{\mathbf{z}}_1, \tilde{\mathbf{z}}_2, \tilde{\mathbf{z}}_3 \in \mathbb{C}^{N_N}$, such that for $i = 1,\ldots N_N$

$$\begin{aligned} a(\mathcal{X}_{\cdot r}^{(\mathbf{x}),h}, \boldsymbol{\varphi}_1^i) &= a\left(\sum_{j=1}^{N_N} z_1^j\,\varphi^j\,\mathbf{e}_1 + z_2^j\,\varphi^j\,\mathbf{e}_2 + z_3^j\,\varphi^j\,\mathbf{e}_3,\ \varphi^i\,\mathbf{e}_1\right) = \sum_{j=1}^{N_N} a\left(z_1^j\,\varphi^j\,\mathbf{e}_1 + z_2^j\,\varphi^j\,\mathbf{e}_2 + z_3^j\,\varphi^j\,\mathbf{e}_3,\ \varphi^i\,\mathbf{e}_1\right) \\ &= \sum_{j=1}^{N_N} z_1^j\,a(\varphi^j\,\mathbf{e}_1,\ \varphi^i\,\mathbf{e}_1) + z_2^j\,a(\varphi^j\,\mathbf{e}_2,\ \varphi^i\,\mathbf{e}_1) + z_3^j\,a(\varphi^j\,\mathbf{e}_3,\ \varphi^i\,\mathbf{e}_1) = \langle \boldsymbol{l}, \boldsymbol{\varphi}_1^i\rangle = \langle \boldsymbol{l}, \varphi^i\,\mathbf{e}_1\rangle. \end{aligned}$$

We remember that we search for $\tilde{\mathbf{z}}_1, \tilde{\mathbf{z}}_2$ and $\tilde{\mathbf{z}}_3$ and that the integrations are executed on $\Omega_\lambda^{(\mathbf{x})}$. This yields starting from (23)

$$\begin{aligned} &\bar{\nu}\int \nabla\left(\sum_{j=1}^{N_N} z_1^j\,\varphi^j\right)\cdot\nabla\varphi^i\,\mathrm{d}\mathbf{x}' + \mathrm{i}\omega\sigma\int\sum_{j=1}^{N_N} z_1^j\,\varphi^j\cdot\varphi^i\,\mathrm{d}\mathbf{x}' \\ &\quad + \int\left\{\tilde{\nu}(\mathbf{x}')\,\mathbf{curl}\left\{\sum_{j=1}^{N_N}\sum_{d=1}^{3} z_d^j\,\varphi^j\,\mathbf{e}_d\right\}\right\}\cdot\{\mathbf{curl}\,\varphi^i\,\mathbf{e}_1\}\,\mathrm{d}\mathbf{x}' = b_{1,r}(\mathbf{x}) \quad \forall i = 1,\ldots,N_N, \end{aligned}$$

where $b_{1,r}(\mathbf{x}) := \int \epsilon_{1pr}\partial_{x'_p}\tilde{\nu}(\mathbf{x}')\varphi^i\,d\mathbf{x}'$. Considering the linearity of **curl curl** and taking advantage of the identity $\mathbf{curl}\,\phi(\mathbf{x})\,\mathbf{a}(\mathbf{x}) = \phi(\mathbf{x})\,\mathbf{curl}\,\mathbf{a}(\mathbf{x}) - \mathbf{a}(\mathbf{x}) \times \nabla\phi(\mathbf{x})$ which holds for scalar functions $\phi(\mathbf{x})$ and vectors $\mathbf{a}$, we obtain $\mathbf{curl}\,z_d^j\varphi^j\,\mathbf{e}_d = -\mathbf{e}_d \times z_d^j\nabla\varphi^j = z_d^j\nabla\varphi^j \times \mathbf{e}_d$ and $\mathbf{curl}\,\varphi^i\,\mathbf{e}_1 = \nabla\varphi^i \times \mathbf{e}_1$. The equation system then reads

$$\int \sum_{j=1}^{N_N} z_1^j[\bar{\nu}\nabla\varphi^j\cdot\nabla\varphi^i + \mathrm{i}\omega\sigma\varphi^j\cdot\varphi^i]\,d\mathbf{x}' + \int \tilde{\nu}(\mathbf{x}')\sum_{j=1}^{N_N}\left\{ z_1^j\begin{pmatrix}0\\ -\partial_3\varphi^j\\ -\partial_2\varphi^j\end{pmatrix} + z_2^j\begin{pmatrix}-\partial_3\varphi^j\\ 0\\ \partial_1\varphi^j\end{pmatrix} + z_3^j\begin{pmatrix}\partial_2\varphi^j\\ \partial_1\varphi^j\\ 0\end{pmatrix}\right\}$$
$$\cdot\begin{Bmatrix}0\\ -\partial_3\varphi^i\\ -\partial_2\varphi^i\end{Bmatrix} d\mathbf{x}' = b_{1,r}(\mathbf{x}) \quad \forall i = 1,\ldots,N_N,$$

and finally

$$\sum_{j=1}^{N_N}\begin{Bmatrix}\int \bar{\nu}\nabla\varphi^j\cdot\nabla\varphi^i + \mathrm{i}\omega\sigma\varphi^j\cdot\varphi^i\,d\mathbf{x}'\\ 0\\ 0\end{Bmatrix}\cdot\begin{Bmatrix}z_1^j\\ 0\\ 0\end{Bmatrix} - \int\tilde{\nu}(\mathbf{x}')\sum_{j=1}^{N_N}\begin{Bmatrix}-z_2^j\partial_3\varphi^j + z_3^j\partial_2\varphi^j\\ -z_1^j\partial_3\varphi^j + z_3^j\partial_1\varphi^j\\ -z_1^j\partial_2\varphi^j + z_2^j\partial_1\varphi^j\end{Bmatrix}\cdot\begin{Bmatrix}0\\ \partial_3\varphi^i\\ \partial_2\varphi^i\end{Bmatrix}d\mathbf{x}'$$
$$= b_{1,r}(\mathbf{x}) \quad \forall i = 1,\ldots,N_N.$$

The equation system can be rewritten as:

Find $(z_d^j)_j$, $d = 1,2,3$, such that for all $i = 1,\ldots,N_N$

$$\sum_{j=1}^{N_N}\begin{Bmatrix}\int\bar{\nu}\nabla\varphi^j\cdot\nabla\varphi^i + \tilde{\nu}(\mathbf{x}')\partial_2\varphi^j\partial_2\varphi^i + \tilde{\nu}(\mathbf{x}')\partial_3\varphi^j\partial_3\varphi^i\,d\mathbf{x}'\\ -\int\tilde{\nu}(\mathbf{x}')\partial_1\varphi^j\partial_2\varphi^i\,d\mathbf{x}'\\ -\int\tilde{\nu}(\mathbf{x}')\partial_1\varphi^j\partial_3\varphi^i\,d\mathbf{x}'\end{Bmatrix}\cdot\begin{Bmatrix}z_1^j\\ z_2^j\\ z_3^j\end{Bmatrix} + \sum_{j=1}^{N_N}\mathrm{i}\omega\sigma\begin{Bmatrix}\int\varphi^j\varphi^i\,d\mathbf{x}'\\ 0\\ 0\end{Bmatrix}\cdot\begin{Bmatrix}z_1^j\\ z_2^j\\ z_3^j\end{Bmatrix} = b_{1,r}(\mathbf{x}). \tag{24}$$

For further simplifications we define the vectors

$$s_1^{ij} := \begin{Bmatrix}\int\bar{\nu}\nabla\varphi^j\cdot\nabla\varphi^i + \tilde{\nu}(\mathbf{x}')\partial_2\varphi^j\partial_2\varphi^i + \tilde{\nu}(\mathbf{x}')\partial_3\varphi^j\partial_3\varphi^i\,d\mathbf{x}'\\ -\int\tilde{\nu}(\mathbf{x}')\partial_1\varphi^j\partial_2\varphi^i\,d\mathbf{x}'\\ -\int\tilde{\nu}(\mathbf{x}')\partial_1\varphi^j\partial_3\varphi^i\,d\mathbf{x}'\end{Bmatrix}$$

and

$$m_1^{ij} := \begin{Bmatrix}\int\varphi^j\varphi^i\,d\mathbf{x}'\\ 0\\ 0\end{Bmatrix}.$$

Analogously, we get the equations for the second and third component. Regarding Eq. (24) it is obvious that the three components of the weighting vector in a node $\mathbf{y}_j$, denoted by z_1, z_2, z_3 are coupled within the equations for the three components of $\mathcal{X}_{\cdot r}$.

Considering a lexicographical numbering of the nodes we choose a point-wise gathering for the unknowns since it leads to smaller blocks compared to an equation-wise aggregation. A node $\mathbf{y}_i$ then is coupled with each of his neighbor nodes $\mathbf{y}_j$ via a complex (3×3)-matrix, and in every node we have to solve the following equation system:

$$\mathbf{S}^{ij}\mathbf{z}^j + \mathrm{i}\mathbf{M}^{ij}\mathbf{z}^j = \mathbf{b}^i \tag{25}$$

with the coupling matrices $\mathbf{S}$ and $\mathbf{M}$ which we will stiffness matrix and mass matrix, respectively.

This notation is adopted from [7] where a discretization of Maxwell's equations with Whitney elements is shown. The mass matrix contains the parts arising from the identity, in the stiffness matrix the remaining parts of the operator – the parts resulting from the Laplacian and the **curl curl** operator – are accumulated. We remark that this is similar when treating Maxwell's equations with Whitney-1-elements, see [7]. The stiffness and mass matrix have the following structure:

$$\mathbf{S}^{ij} = \begin{pmatrix} (s^{1,ij})^t \\ (s^{2,ij})^t \\ (s^{3,ij})^t \end{pmatrix} \quad \text{and} \quad \mathbf{M}^{ij} = \begin{pmatrix} (m^{1,ij})^t \\ (m^{2,ij})^t \\ (m^{3,ij})^t \end{pmatrix}$$

where $(\cdot)^t$ denotes the transpose.

4.4. Right-hand side

Next we consider the right-hand side which depends on r. As the fluctuations $v(\mathbf{x}')$ are non-continuous functions on $\Omega_\lambda^{(\mathbf{x})}$, we have to apply a partial integration for b_1, b_2, b_3. Depending on the choice of boundary conditions we have to separate two cases:

If we choose Dirchilet boundary conditions $\mathcal{X}_{\cdot r}^{(\mathbf{x})}(\mathbf{x}') = 0$, the test functions φ vanish on the boundary of $\Omega_\lambda^{(\mathbf{x})}$, and therefore the boundary terms of a partial integration as well. At the ith node $\mathbf{y}_i$ the kth component yields for with fixed p

$$b_{k,r}(\mathbf{x}) = \int_{\Omega_\lambda^{(\mathbf{x})}} \epsilon_{kpr}\, \partial_{x'_p} \tilde{v}(\mathbf{x}')\, \varphi^i(\mathbf{x}')\, \mathrm{d}^3x' = -\int_{\Omega_\lambda^{(\mathbf{x})}} \epsilon_{kpr}\, \tilde{v}(\mathbf{x}')\, \partial_{x'_p} \varphi^i(\mathbf{x}')\, \mathrm{d}^3x'.$$

Obviously the right-hand side varies with the row index k and the column index r, and it vanishes for $k = r$.

Using the boundary conditions $\mathbf{n}(\mathbf{x}') \times \mathcal{X}_{\cdot r}^{(\mathbf{x})}(\mathbf{x}') = 0$, the test functions do not vanish on the boundary and the right-hand side becomes

$$\int_{\Omega_\lambda^{(\mathbf{x})}} \epsilon_{kpr}\, \partial_{x'_p} \tilde{v}(\mathbf{x}')\, \varphi^i(\mathbf{x}')\, \mathrm{d}^3x' = -\int_{\Omega_\lambda^{(\mathbf{x})}} \epsilon_{kpr}\, \tilde{v}(\mathbf{x}')\, \partial_{x'_p} \varphi^i(\mathbf{x}')\, \mathrm{d}^3x' + \iint_{\Omega_\lambda^{(\mathbf{x})}} \tilde{v}(\mathbf{x}')\, \varphi^i|_{x'_p=0}^{x'_p=1}\, \mathrm{d}x'_v\, \mathrm{d}x'_w,$$

where the indices v and w have to differ from the fixed index p which is the direction of the one-dimensional partial integration. In each component we have to integrate over element-wise constant functions, so the Midpoint rule renders exact results.

4.5. Decoupling real and imaginary part

For the numerical computation we have to decouple the complex equation system (25) for the unknown weights z_1^j, z_2^j, z_3^j into real and imaginary part. This can be done analogously to the case of Whitney elements, see e.g. [29]. Let $\mathbf{z}^j = \mathbf{u}^j + \mathrm{i}\mathbf{v}^j$. Then

$$\begin{aligned} \mathbf{S}^{ij}\{\mathbf{u}+\mathrm{i}\mathbf{v}\}^j + \mathrm{i}\mathbf{M}^{ij}\{\mathbf{u}+\mathrm{i}\mathbf{v}\}^j = \mathbf{b}_{\mathrm{re}}^i + \mathrm{i}\,\mathbf{b}_{\mathrm{im}}^i &\iff \mathbf{S}^{ij}\{\mathbf{u}\}^j - \mathbf{M}^{ji}\{\mathbf{v}\}^j + \mathrm{i}\,[\mathbf{M}^{ij}\{\mathbf{u}\}^j + \mathbf{S}^{ij}\{\mathbf{v}\}^j] = \mathbf{b}_{\mathrm{re}}^i + \mathrm{i}\,\mathbf{b}_{\mathrm{im}}^i \\ &\iff \begin{pmatrix} \mathbf{S} & -\mathbf{M} \\ \mathbf{M} & \mathbf{S} \end{pmatrix}_{6\times 6}^{ij} \begin{Bmatrix} \mathbf{u} \\ \mathbf{v} \end{Bmatrix}^j = \begin{Bmatrix} \mathbf{b}_{\mathrm{re}} \\ \mathbf{b}_{\mathrm{im}} \end{Bmatrix}^i, \end{aligned}$$

and two domain nodes $\mathbf{y}_i$ and $\mathbf{y}_j$ are coupled with the following (6×6)-matrix:

$$\left(\begin{array}{ccc:ccc} s_{11} & s_{12} & s_{13} & -m_{11} & 0 & 0 \\ s_{21} & s_{22} & s_{23} & 0 & -m_{22} & 0 \\ s_{31} & s_{32} & s_{33} & 0 & 0 & -m_{33} \\ \cdot & \cdot & \cdot & \cdot & \cdot & \cdot \\ +m_{11} & 0 & 0 & s_{11} & s_{12} & s_{13} \\ 0 & +m_{22} & 0 & s_{21} & s_{22} & s_{23} \\ 0 & 0 & +m_{33} & s_{31} & s_{32} & s_{33} \end{array}\right)_{6\times 6}^{ij}$$

where the first three rows exhibit the real part, the last three yield the imaginary part of the system.

On the diagonal of this matrix we find the parts of the Laplacian as well as the parts of the Laplacian part of **curl curl**, i.e., **curl curl** $= -\triangle +$ **grad** div in three dimensions:

$$s_{kk} = \int_{\Omega_\lambda^{(\mathbf{x})}} \left(\bar{\nu} \nabla \varphi^i \cdot \nabla \varphi^j + \tilde{\nu}(\mathbf{x}') \sum_{l=1}^{3} (1 - \delta_{kl}) \, \partial_l \varphi^i \, \partial_l \varphi^j \right) \mathrm{d}\mathbf{x}'.$$

The outer diagonal elements of S contain the **grad** div parts of **curl curl**:

$$s_{kl} = \int_{\Omega_\lambda^{(\mathbf{x})}} \partial_k \varphi^i \, \partial_l \varphi^j,$$

and on the diagonal of M the parts resulting from the identity,

$$m_{kk} = \omega\sigma \int_{\Omega_\lambda^{(\mathbf{x})}} \varphi^i \cdot \varphi^j.$$

In the stiffness matrices $\mathbf{S}$, we need to execute integrations over derivatives of linear functions. For these are constant we can apply the Midpoint rule again. In the mass matrices $\mathbf{M}$ a quadrature formula has to be used since we have to integrate over the product of two element-wise linear functions.

4.6. Calculation of $\delta\nu^{\mathrm{eff}}$ from $\mathcal{X}$

After calculating all weights in all nodes, we obtain the reluctivity tensor from (16) using the basis (22). Exemplary we state the results for the first component with fixed column index r:

$$\begin{aligned}
\delta\nu_{1r}^{\mathrm{eff}} &= \int_{\Omega_\lambda^{(\mathbf{x})}} \epsilon_{123} \, \tilde{\nu}(\mathbf{x}') \, \partial_{x_2'} \left(\sum_{j=1}^{N_N} z_3^j \varphi^j \right) + \epsilon_{132} \, \tilde{\nu}(\mathbf{x}') \, \partial_{x_3'} \left(\sum_{j=1}^{N_N} z_2^j \varphi^j \right) \mathrm{d}^3 x' = \int_{\Omega_\lambda^{(\mathbf{x})}} \tilde{\nu}(\mathbf{x}') \sum_{j=1}^{N_N} \left(z_3^j \partial_{x_2'} \varphi^j - z_2^j \partial_{x_3'} \varphi^j \right) \mathrm{d}^3 x' \\
&= \int_{\Omega_\lambda^{(\mathbf{x})}} \tilde{\nu}(\mathbf{x}') \sum_{j=1}^{N_N} [(u_3^j \partial_{x_2'} \varphi^j - u_2^j \partial_{x_3'} \varphi^j) + \mathrm{i} \, (v_3^j \partial_{x_2'} \varphi^j - v_2^j \partial_{x_3'} \varphi^j)] \, \mathrm{d}^3 x',
\end{aligned}$$

with the real parts u_2, u_3 and imaginary parts v_2, v_3 of the complex weights z_2, z_3. The steps for the second and third component are analogous.

4.7. Solving Maxwell's equations

So far we have shown the numerical treatment for the Coarse Graining sub-problems. Using the effective reluctivity tensors from the Coarse Graining method, we moreover have to solve the Maxwell-problem (2). The latter does not include the Laplacian, so the numerical treatment is completely different.

We would like to remark that in the case of solving the standard Maxwell Eq. (2) we choose in Section 5 a standard FEM with a variational formulation over the space $\mathbf{H}(\mathbf{rot}; \Omega)$ and a basis of Whitney-1-elements, as it is done, e.g. in Refs. [29,7], and set appropriate boundary conditions. We refer the reader to [29] for a detailed description of the discretization and the iterative methods useful to solve problem (2).

5. Numerical results

In this section we present the numerical results for the effective reluctivity tensors computed by the discretization of Section 4. We compare the numerical results with the results of the perturbation theory. Therefore we average the numerical tensors over the domain to obtain space-independent scalar permeability fields on the coarser scale. We also show how some characteristics of the Maxwell problem such as the Ohmic losses and the $\mathbf{L}^2$-norm of the solution scale when upscaling to larger length scales. The numerical discretization is implemented in the simulation toolbox *UG*, see [4,5].

In order to solve the discrete equation system (23) for the columns of $\mathcal{X}$, we choose a standard linear multigrid method. As a pre- and post-smoother we apply a Gauss–Seidel and execute a $V(1,1)$-cycle. The

hierarchy of grids is given by $\mathcal{T}^l$, which was introduced in 4.2. We choose the grid for the Coarse Graining Blocks fine enough that the reluctivity is always constant on each element of the discretization grid.

5.1. Comparison of the results for different boundary conditions

On the unit cube we provide a permeability field with $64 \times 64 \times 64$ cells. For each experiment the field has a mean value of $\bar{\mu} = 2.0$ and a variance of $\sigma^2 = 0.1$. For the reluctivity field we thus obtain a mean $\bar{\nu} = 0.5137$ and a variance $q_0 = 0.0079$, using an ensemble of ten realizations. The correlation length is $l_0 = 0.03125$.

Fig. 1 left shows the numerical results of the first and third components v_{11} and v_{33} of the effective reluctivity tensor in comparison with the theoretical value given by (10) as a function of the scale λ/l_0. The numerical results are computed for $\mathbf{n} \times \mathcal{X}_{\cdot r} = 0$ boundary conditions. The results show a quite good conformance with a significant deviation for an upscaling to scales λ with $\lambda/l_0 \approx 8$.

Fig. 1 right displays the numerical results for Dirichlet boundary conditions $\mathcal{X}_{\cdot r} = 0$ for the columns of $\mathcal{X}$. Again we rerun the experiment 10 times. We remark that the choice of the boundary conditions does not seem to have great impact to the solution of the problem. We explain about this as follows. Using boundary conditions $\mathcal{X}_{\cdot r} = 0$ corresponds to a discretization of the Coarse Graining problems with $\mathbf{H}_0^1$-conforming Finite Elements, the second type of boundary condition implies a discretization over $\mathcal{W} = \{\mathbf{v} \in \mathbf{H}^1; \mathbf{n} \times \mathbf{v} = 0 \text{ on the boundary.}\}$. We remark $\mathbf{H}_0^1$ is a subspace of $\mathcal{W}$, but for complex domains both spaces coincide, as explained in Section 4. Furthermore the Laplacian dominates the equation. Hence we guess that the approximation leads to a solution in $\mathbf{H}_0^1$, which coincides with the solution in $\mathcal{W}$.

For the given experimental setup we examine the scale-dependent behavior of two quantities in order to estimate the quality of an upscaling with the Coarse Graining method. We choose the $\mathbf{L}^2$-norm of the solution $\mathbf{E}$ and the Ohmic loss. The loss is the energy which is transformed into heat and has to be compensated by the generator with its current $\mathcal{J}^G$. For both quantities we define as values of the finest scale on the scale $\lambda = 0$ with the scalar reluctivity field. The Ohmic losses are in physics defined by $P_{\text{Ohm}} := \frac{1}{2}\int_\Omega \sigma |\mathbf{E}|^2 \, d\mathbf{x}$, see [19]. We then solve Maxwell problem (8) on different scales and compute the two quantities. Table 1 shows the relative progression of the $\mathbf{L}^2$-norm of the solution $\mathbf{E}$ and the Ohmic losses over scales λ/l_0. For an upscaling to minor scales we see a deviation of about 10%. That means that the Coarse Graining method here is not able to repro-

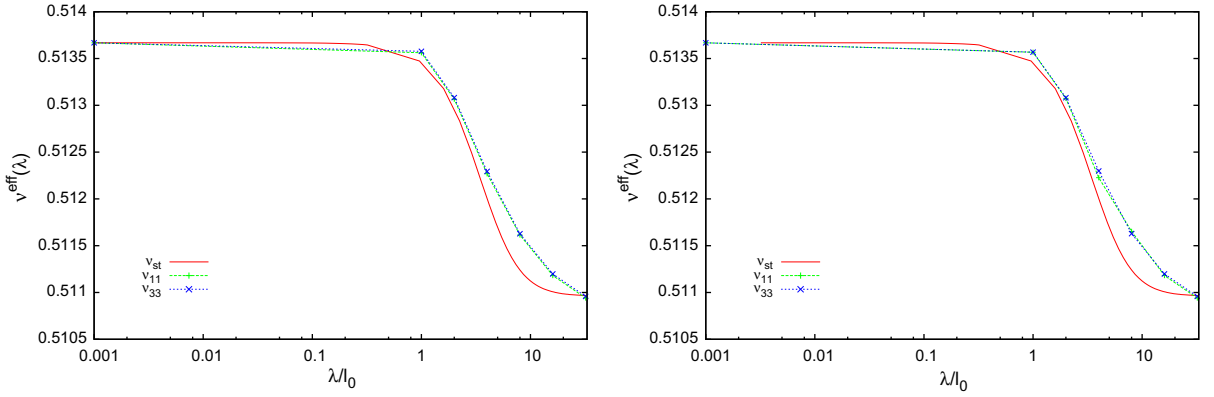

Fig. 1. Comparison of the scale-dependent behavior of $\nu_{\text{st}}^{\text{eff}}$ from perturbation theory and ν^{num} from numerical simulations for a reluctivity field with $\bar{\nu} = 0.5137$ and $q_0 = 0.0079$ with $\mathbf{n} \times \mathcal{X}_{\cdot r} = 0$ (left side) and $\mathcal{X}_{\cdot r} = 0$ (right side) as boundary conditions.

Table 1
Scale-dependent behavior of the L^2-error and the total Ohmic losses regarding an upscaling to various resolution scales

λ/l_0	1.0	2.0	3.0	4.0	8.0	16	32
$\|\mathbf{E}\|_{L_2}$	1	0.900	0.918	0.932	0.918	0.937	0.936
P_{Ohm}	1	0.891	0.913	0.929	0.925	0.937	0.938

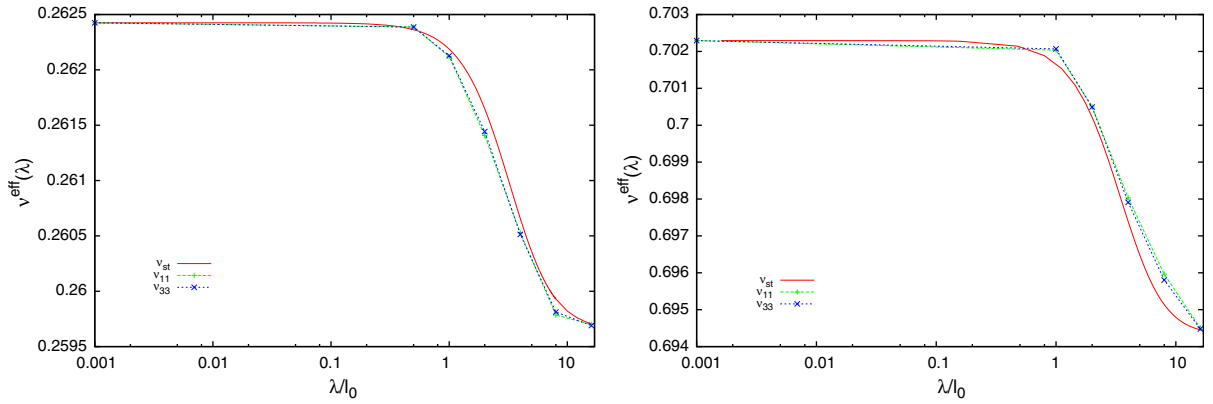

Fig. 2. Comparison of the scale-dependent behavior of ν_{st}^{eff} from perturbation theory and ν^{num} from numerical simulations for a reluctivity field with $\bar{\nu} = 0.262$ and $q_0 = 0.015$ (left side) and a field with $\bar{\nu} = 0.702$ and $q_0 = 0.033$ (right side). For both simulations boundary conditions $\mathcal{X}_{,r} = 0$ have been chosen.

duce the influences of sub-scale fluctuations. But for an upscaling to larger scales the deviation decreases under 6%, what can be considered as a very good result.

5.2. Computations for different reluctivity fields

Here we will show the effective reluctivities for different heterogeneous materials. We use fields with $\bar{\mu} = 4.0$ and $\sigma^2 = 0.7$ and with $\bar{\mu} = 1.5$ and $\sigma^2 = 0.1$. For the first field we obtain $\bar{\nu} = 0.262$ and $q_0 = 0.015$ for reluctivity field, for the second the values are $\bar{\nu} = 0.702$ and $q_0 = 0.033$.

In both simulations the isotropic correlation length is $l_0 = 0.125$ and we set $\mathcal{X}_{,r} = 0$ on the boundary. The experiments are repeated 10 times. The results from theory and simulations are shown in Fig. 2 for the first setup and in Fig. 2 for the second. Both simulations show good accordance between the theoretical and numerical results for the effective reluctivity tensors.

6. Conclusion

The paper studies a numerical upscaling of the eddy-current approximation of the Maxwell equations for heterogeneous media using the Coarse Graining method. The magnetic permeability of the heterogeneous media is treated by a stochastic modeling. We apply the Coarse Graining method to develop a numerical upscaling of the eddy-current model which results in effective reluctivity tensors. The latter are scale- and space-dependent and model the influence of sub-scale fluctuations in the upscaled eddy-current model. Eberhard [11] derived a perturbation theory to compute the reluctivity tensors and showed that they could be computed numerically by solving local partial differential equations.

In particular, we address the numerical computation of the effective reluctivity tensors solving the local differential equations. These equations are made up of the Laplacian and curl–curl operator for the electric field. To our knowledge the so combined operator has not yet been analyzed in the literature – neither in theory nor in numerical approaches. We present a discretization of this operator on convex domains based on an extension of the standard variational formulation for the Laplacian in three spatial dimensions. The resulting discrete equation system can be divided into real- and imaginary part. As appropriate boundary conditions we choose either zero Dirichlet boundary conditions or $\mathbf{n} \times \mathcal{X}_{,r} = 0$. Both conditions result in very similar numerical results. We remark that in general the assembling of the system matrix is analogous to the case of the discretization of Maxwell's equations by Whitney-1-elements or by a nodal approach for a vector potential formulation.

We numerically solve the arising system of equations by a standard multigrid method. Comparing the numerical results with the results of the perturbation theory we observe a very good agreement. Moreover, using

the effective reluctivities in the upscaled eddy-current model we obtain a very similar system behavior compared to the fine-scale model in terms of the L^2-error and the total Ohmic losses along with less computational effort. In the future, we would like to extend the Coarse Graining method to tensor fields in order to enhance an iterative upscaling of the fields. It would be also interesting to study the numerical upscaling for non-convex domains to access practical applications. Further, it could be of interest to analyze the Coarse Graining method as a grid transfer in a multigrid method for Maxwell's equations as done for flow problems in [14].

References

[1] M. Abramowitz, A. Stegun, Handbook of Mathematical Functions, Dover Publications, New York, 1972.
[2] S. Attinger, Generalized coarse graining procedures for flow in porous media, Computational Geosciences 7 (2003) 253–273.
[3] S. Attinger, J.P. Eberhard, N. Neuss, Filtering procedures for flow in heterogeneous porous media: numerical results, Computing and Visualization in Science 5 (2002) 67–72.
[4] P. Bastian, K. Johannsen, S. Lang, N. Neuss, H. Rentz-Reichert, C. Wieners, UG – a flexible software toolbox for solving partial differential equations, Computing and Visualization in Science 1 (1997) 27–40.
[5] P. Bastian, K. Johannsen, S. Lang, V. Reichenberger, C. Wieners, G. Wittum, C. Wrobel, A parallel software-platform for solving problems of partial differential equations using unstructured grids and adaptive multigrid methods, in: W. Jäger, E. Krause (Eds.), High Performance Computing in Science and Engineering, Springer, 1999, pp. 326–339.
[6] A. Bossavit, On the homogenization of Maxwell equations, COMPEL – The International Journal of Computation an Mathematics in Electrical and Electronic Engineering 14 (4) (1996) 23–26.
[7] A. Bossavit, Computational Electromagnetism. Variational Formulation, Complementary, Edge Elements, second ed., Academic Press, San Diego, 1998.
[8] M. Costabel, A coercive bilinear form for Maxwell's equations, Journal of Mathematical Analysis and Applications 157 (2) (1991) 527–541.
[9] M. Costabel, M. Dauge, Singularities of electromagnetic fields in polyhedral domains, Archive for Rational Mechanics and Analysis 151 (3) (2000) 221–276.
[10] M. Dorobantu, B. Engquist, Wavelet-based numerical homogenization, SIAM Journal on Numerical Analysis 35 (2) (1998) 540–559.
[11] J.P. Eberhard, Upscaling for the time-harmonic Maxwell equations with heterogeneous magnetic materials, Physical Review E 72 (3) (2005).
[12] J.P. Eberhard, Simulation of lognormal random fields with varying resolution scale and local average for darcy flow, Computing and Visualization in Science 9 (2006) 1–10.
[13] J.P. Eberhard, S. Attinger, G. Wittum, Coarse graining for upscaling of flow in heterogeneous porous media, Multiscale Modelling and Simulations 2 (2) (2004) 269–301.
[14] J.P. Eberhard, G. Wittum, A coarsening multigrid method for flow in heterogeneous porous media, in: B. Engquist, P. Lötstedt, O. Runborg (Eds.), Multiscale Methods in Science and Engineering, Lecture Notes in Computational Science and Engineering, vol. 44, Springer, Berlin, Heidelberg, 2005, pp. 111–132.
[15] M. El Feddi, Z. Ren, A. Razek, A. Bossavit, Homogenization technique for Maxwell equations in periodic structure, IEEE Transactions on Magnetics 33 (2) (1997) 1382–1386.
[16] F.G. Friedlander, Introduction to the Theory of Distributions, Cambridge University Press, Cambridge, 1982.
[17] L.W. Gelhar, Stochastic Subsurface Hydrology, Prentice-Hall, New Jersey, 1993.
[18] W. Hackbusch, Elliptic Differential Equations, third ed., Springer, Berlin, 1992.
[19] J.D. Jackson, Classical Electrodynamics, third ed., John Wiley & Sons, Inc, New York, 1999.
[20] V.V. Jikov, S.M. Kozlov, O.A. Oleinik, Homogenization of Differential Operators and Integral Functionals, Springer, Berlin, 1994.
[21] J. Jin, The Finite Element Method in Electromagnetics, John Wiley & Sons, Inc., New York, 1993.
[22] R.H. Kraichnan, Diffusion by a random velocity field, Physics of Fluids 13 (1970) 22–31.
[23] G. Kristensson, Homogenization of the Maxwell equations in an anisotropic material, Radio Science 38 (2) (2003).
[24] G. Kristensson, N. Wellander, Homogenization of the Maxwell equations at fixed frequency, SIAM Journal of Applied Mathematics 64 (1) (2003) 170–195.
[25] W.D. MacComb, The Physics of Fluid Turbulence, Clarendon Press, Oxford, 1994.
[26] V. Mazet, D. Brie, J. Idier, Simulation of positive normal variables using several proposal distributions, In IEEE Workshop on Statistical Signal Processing, Bordeaux, 2005, pp. 37–42.
[27] P. Monk, Finite Element Methods for Maxwell's Equations, first ed., Oxford University Press, New York, 2003.
[28] Y. Niibori, T. Chida, The use of standard deviation and skewness for estimating apparent permeability in a two-dimensional, heterogeneous medium, Transport in Porous Media 15 (1) (1994) 1–14.
[29] O. Sterz, A. Hauser, G. Wittum, Adaptive local multigrid methods for solving time-harmonic eddy-current problems, IEEE Transaction on Magnetics 42 (2) (2006) 309–318.
[30] C. Tai, Dyadic Green's Function in Electromagnetic Theory, Intext Educational Publishers, Scranton, 1971.
[31] A.P. Vinogradov, V. Aivazyan, Scaling theory for homogenization of the Maxwell equations, Physical Review E 60 (1) (1999) 987–993.
[32] K. Yosida, Functional Analysis, sixth ed., Springer, Berlin, Heidelberg, New York, 2003.